Optical and Quantum Electronics (2024) 56:1276
https://doi.org/10.1007/s11082-024-07190-0

# Synthesis of Azo-BE: nonlinear optical properties studies at visible, cw, laser beams

**Uhood J. Al-Hamdani[1] · Qusay M. A. Hassan[2] · Ayat K. Hashim[1] · H. A. Sultan[2] · T. A. Alsalim[2] · C. A. Emshary[2]**

Received: 19 April 2024 / Accepted: 13 June 2024


**Abstract**
4-((6-Methylbenzo[d]thiazol-2-yl)diazenyl)phenyl 4-chlorobenzoate(Azo-BE) is synthesized and characterized using $^{1}$HNMR and $^{13}$CNMR, mass spectra, differential scanning calorimetry, optimized structure and calculation of HOMO (H) and LUMO (L) and gap energy. The Azo-BE nonlinear optical properties using cw laser beam of wavelength 473 nm are studied. The nonlinear refraction index, $n_2$, of Azo-BE is calculated using the same wavelength via the diffraction patterns and Z-scan. $n_2$ value of $3.121 \times 10^{-11}$ $m^2/W$ is obtained. It appears that Azo-BE bare no nonlinear absorption coefficient, β, at 473 nm beam and power input used. All optical switching, static and dynamic, are tested in Azo-BE using 473 and 532 nm laser beams.

**Keywords** Azo-BE · Optical nonlinearities · Diffraction patterns · Z-scan · All-optical switching

## 1 Introduction

To achieve the requirements of progress in photonic applications and in the manufacture of optical devices, we need materials that possess high nonlinear optical (NLO) properties. During the past thirty years, researchers have tested many materials, such as phthalocyanine (Kadhum et al. 2018; Hassan et al. 2019), curcumin derivatives (Sultan et al 2018; Elias et al. 2018; Saeed et al. 2020; Tuma et al. 2023; Adil et al. 2023), Schiff bases (Almashal et al. 2020; Jassem et al. 2021a; Salim et al. 2022), azo compounds (Jassem et al. 2021b; Sultan et al. 2021; Mutlaq et al 2021; Dhumad et al. 2021a,b; Hassan et al. 2022), dye doped polymer film (Deepa et al. 2024), acid blue 129 dye doped polymer (Jeyaram 2024a), silicon carbide doped PVA nanocomposites (Parkash et al. 2022), natural pigment curcumin extracted from curcuma longa (Deepa

✉ Qusay M. A. Hassan
qusayali64@yahoo.co.in

[1] Department of Chemistry, College of Education for Pure Sciences, University of Basrah, Basrah 61001, Iraq

[2] Department of Physics, College of Education for Pure Sciences, University of Basrah, Basrah 61001, Iraq

Published online: 02 July 2024

et al. 2023), and dye (Jeyaram 2021a, b; Vinitha et al. 2008) which showed high NLO properties. Despite the many materials that have been found, the search for other materials that possess higher NLO properties than the previously found materials continues until today.

Liquid crystals (LCs) represent middle state between regular crystalline solid state and regular, irregular liquid state. In the first, particles restricted in movement and have a three dimesional geometric system and in the second, particles of a substance move randomly. LCs were discovered by Friedrich Reineters 1988 (Mitov 2014) and received intense interest by the Russian groups led by Zolotko (Zolot'ko et al. 1980, 1995) during the period 1980–1994. LCs studied in various disciplines such as in photoisomerization of azo-dyes (Janossy et al. 1998), in new photo active polymer (Zhao 2014), in LCs polymers (Bighan 2018), in chemical applications (Aljamali et al. 2021), in photonic applications (Beeckman et al. 2011), in optical cells (Sierakowski 1994), in photoresponsive shape memory azobenzene (Wen et al. 2020), in display applications (Castellano 1990), in drugs (Bunjes et al. 2005; Rajak et al. 2019), in pharmaceutical applications (Wee et al. 2012), based on azo-dye—doped switchable gratings (Lin et al. 2009), etc. NLO properties of many LCs have been studied since 1981, diffraction patterns (DPs) were induced by lasers (Durbin et al 1981), the LC nonlinear optics was studied in 1994 (Khoo 1994), the NLO response in 2000 (Lukishova 2000), Z-scan experiments were conducted in 2002 on lyotropic LCs (Cuppo et al. 2002; Gomez et al. 2003), index of refraction (IR) electrical and dispersion properties in carbon-balls' doped nematic LCs were studied too (Okutan et al. 2005). Self-phase modulation (SPM) due to laser beam in nematic LCs and dc applied electric field effects were studied too (Song et al. 2006). Sudan LC NLO response was studied via moiré deflectometry and Z-scan techniques was studied too (Ara et al. 2008), SPM and ring pattern observed- by electrical field applied on LC dye-doped (Ara et al. 2004), NLO investigation of laser beam propagation in dye-nematic LC (Mousavi et al. 2010), optical and geometrical characterization of nonlinear supramolecular LC complexes (Ahmed et al. 2020), new self-organized materials and polymorphic phases of their mixtures investigation (Alrefaee et al. 2022), thermal and NLO properties and all-optical switching (AOS) in LC (Al-Hamdani et al. 2022c, 2023).

In the present work-((6-methylbenzo[d]thiazol-2-yl)diazenyl)phenyl 4-chlorobenzoate (Azo-BE) is synthesized and diagnosed via $^{1}$H and $^{13}$CNMR, DSC, optimized structure, and HOMO (H), LUMO (L) calculations. The NLO properties of the Azo-BE were studied via the diffraction patterns (DPs) and Z-scan using cw, visible, laser beam. All-optical switching (AOS) was tested in Azo-BE using two cw, visible laser beams.

## 2 Experimental

### 2.1 Synthesis procedure of azo compound

Sodium hydroxide solution (20 ml, 1 M) in bath of ice, mixed with 4-hydroxy phenol. The mixture was slowly added to the reaction mixture (8 ml of 3 M HCl, 10 ml of NaNO2, and 10 mmol of 2-Amino-6-methyl benzothiazole) at 0 °C degrees. Orange–colored crystals (azo–dyes) formed after 15 min, filtered, and washed with cold distilled water (Al-Hamdani et al. 2010, 2021a).

### 2.2 Synthesis of ester (Azo-BE)

Equimolar Azo, DCC, 4-Chloro benzoic acid, and Dimethyl amino pyridine were dissolved in dry dichloromethane. The reaction mixture was continuously stirred for 24 h at RT. The mixture was filtered and the solvent was evaporated to obtain an orange (Azo-BE) precipitate, then recrystallized from ethanol (Al-Hamdani et al. 2021b, 2022a, 2022b). The synthesis route of Azo-BE is shown in Fig. 1

### 2.3 Characterization of Azo-BE

Chemical formula: $C_{21}H_{14}ClN_3O_2S$, orange solid; yield 40%,$^{1}$HNMR δ: 2.53 ppm (t, 3H, methyl group), 7.26–8.17 ppm (11 H, H-aromatic) Fig. 2. $^{13}$CNMR δ: 21.9 ppm ($CH_3$), 122.0–174.6 ppm (18 aromatic carbon) Fig. 3; MS (m/z) 407.05[$M^+$] Fig. 4. The IR spectrum (Fig. 5) revealed that the functional groups were in the expected locations. The spectrum displays two bands at 3019 and 2951 $cm^{-1}$ attributed to the vibration of aromatic C-H and aliphatic C-H respectively. The strong band of the carbonyl group of ester C=O at 1743 $cm^{-1}$, and the band at 1591 $cm^{-1}$ attributed to N=N. The band at 1494 $cm^{-1}$ is attributed to the C=C vibration. We notice the disappearance of the band of the OH group for the Azo compound due to condensation with the carboxylic group of 4-Chloro benzoic acid to give the ester group ( ).

### 2.4 Experimental details

Two types solid state lasers emitting 473 and 532 nm beams of powers of 0–60 mW and 0–50 mW both having 1.5 mm (at $e^{-2}$) spot size as they leaves the laser devices were used. Each beam having $TEM_{00}$ transverse distribution. Two 30 × 30 cm and 60 × 60 screens semitransparent used to cast the DPs that resulted when the laser beam pass the sample and registered using digital of exposure time of 1/32 s camera. The beam 473 nm fall on the sample will have a spot size of 19. 235 µm. The Rayleigh length of the laser beam of wavelength 437 nm equals 2.456 mm. To measure the power output, a power meter was used. For a Gaussian laser beam of power input P = 54 mW, its intensity at the lens focus can be calculated using the relation $I = \frac{2P}{\pi\omega_o^2}$ so that I = 9296.3 W/cm$^2$.

In the Z-scan techniques, a translation stage was used to sweep the sample in a glass, l mm cell a distance (−z)–(+z) passing the lens focus (z = 0). A covered power meter with 2 mm diameter iris to secure the stander Z-scan was used.

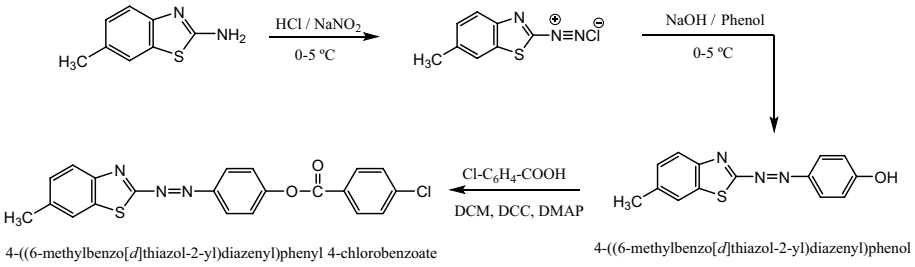


**Fig. 1** Synthesis routes of Azo-BE compound

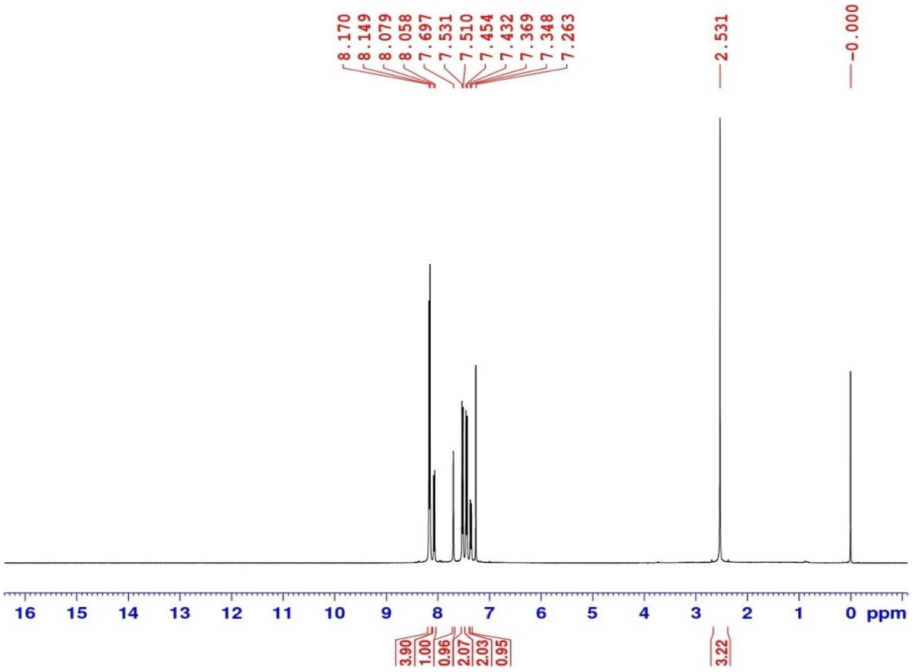


**Fig. 2** [1]HNMR spectrum for Azo-BE

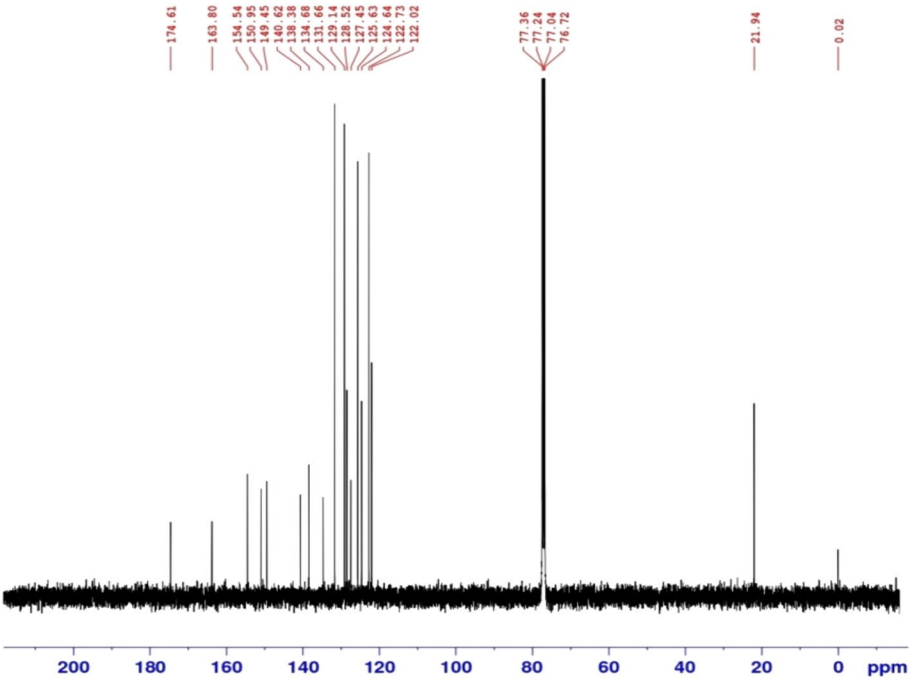


**Fig. 3** [13]CNMR spectrum for Azo-BE

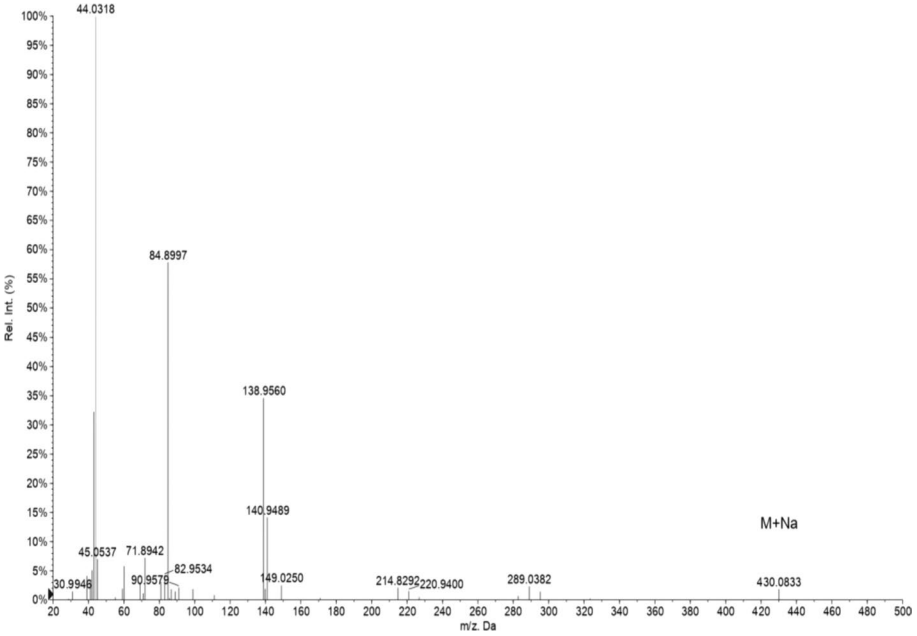


**Fig. 4** Mass spectrum for Azo-BE

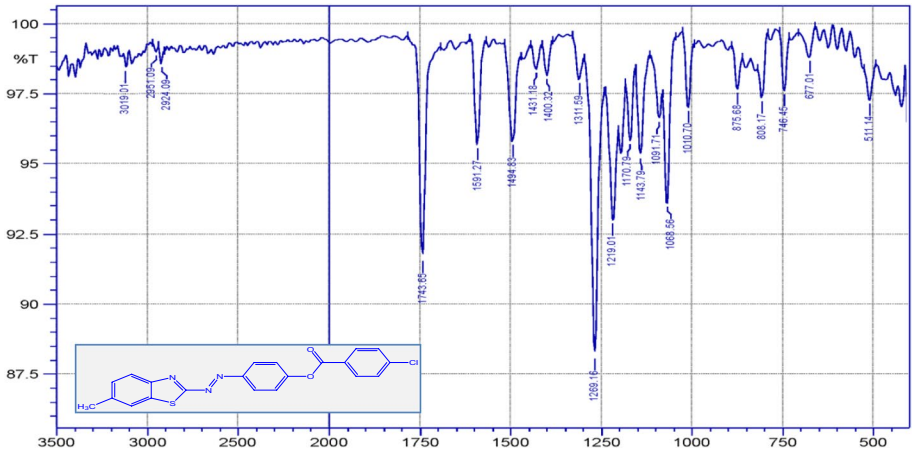


**Fig. 5** Infrared spectrum for Azo-BE

The two lasers were used in the all-optical switching technique having 20 cm focal length lenses to focus the two beams on the sample. The two beams in sample cell will have spot sizes of 76.941 μm (for $\lambda = 473$ nm) and 86.539 nm (for $\lambda = 532$ nm). The generated DPs were casted on the $60 \times 60$ cm semitransparent screen. Figures 6, 7 and 8 shows the main experiments conducted viz.

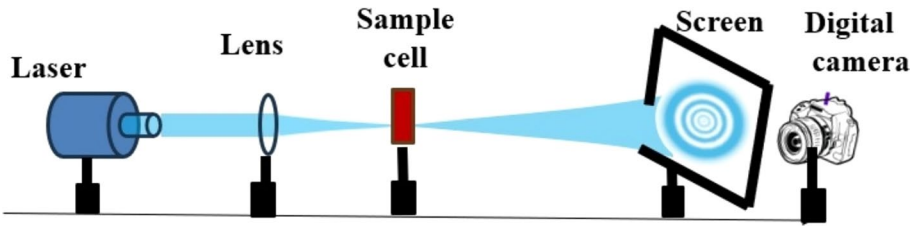


**Fig. 6** Experimental arrangement for obtaining DPs

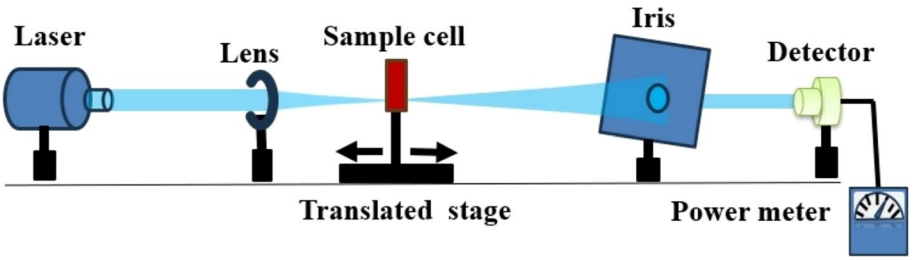


**Fig. 7** Experimental arrangement for studying the Z-scan

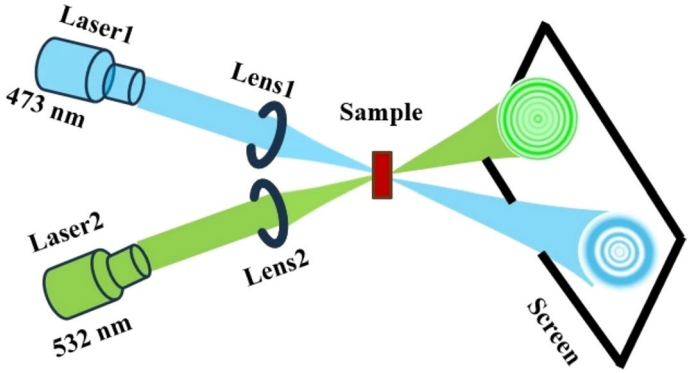


**Fig. 8** Experimental arrangement for obtaining AOS

DPs, Z-scam and AOS. To change the cw behavior of the 473 nm laser beam to pulsed (square) the laser head was connected to a frequency generator.

Optical limiting (OL) in an important application of nonlinear optics. It is used for the protection of optical devices such as the human eye. Good OL strongly attenuates laser beam while exhibiting high transmittance for low-intensity light. Such experiment was conducted by fixing the sample cell at the valley position of the Z-scan when the nonlinear medium nonlinear refractive index is negative. The transmitted light beam power measured with a power meter covered with circular iris. When the beam power fall on the sample is low no nonlinear effect occur so that all the beam pass through the medium. For higher power input nonlinearity sets in so that the relation between the

transmitted beam and the incident one is nonlinear. For even higher power input the beam area exceeds that of the iris so that most of the beam missed the detector.

## 3 Results

### 3.1 Azo-BE thermodynamic properties of

The Azo-BE was studied using a polarized optical microscope (POM) where it was found that the compound LC, as it showed the nematic phase only and turned into a liquid state. The results of the study used microscope agreed with the results of the scanning differential calorimetry (SDC), where the analysis included two peaks (Fig. 9). First peak is due to the transition between the solid state and the nematic phase at 208.01 °C, the second was related to the transition to the isotropic state from nematic phase at 270 °C. The POM shows the texture forms of the nematic phase. The heating of the nematic phase in the Azo-BE compound gives a Marbled texture, while the cooling took the form of Schlieren (Fig. 10).

### 3.2 Computational results

DFT/B3LYP with the 6-311+G(d, p) basis set was used for all theoretical computations. Optimized structures and atomic labeling of synthesized compound are shown in Fig. 11. The figure illustrates the geometrical optimization yield, HOMO–LUMO orbital, and electrostatic potentials surfaces ESP for the non-planar structure.

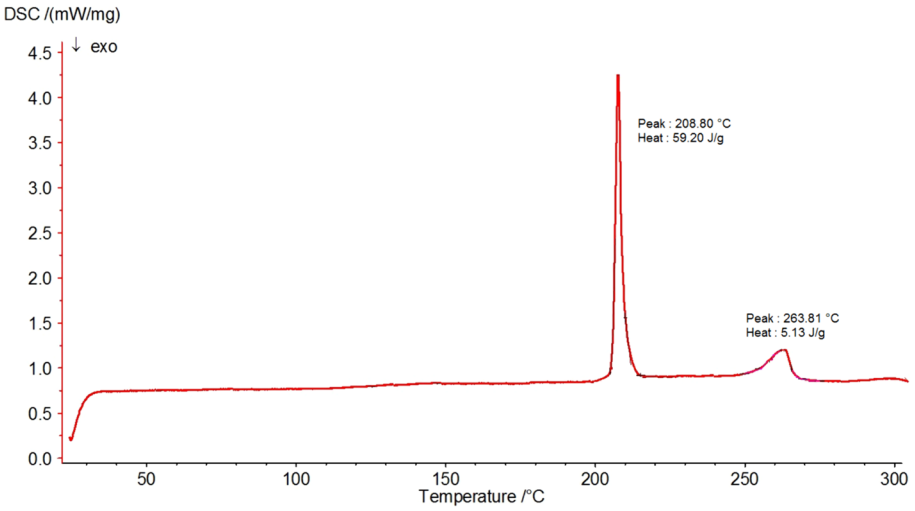


**Fig. 9** DSC thermogram for Azo-BE

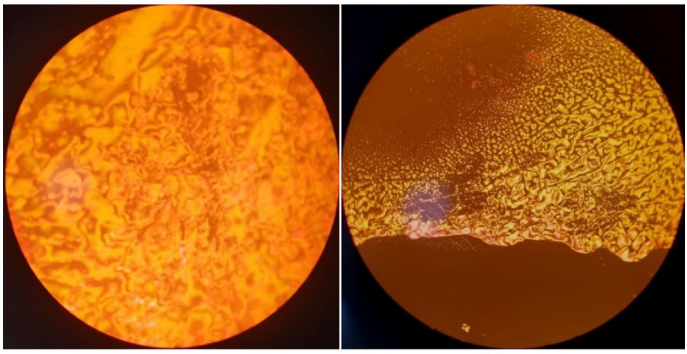


**Fig. 10** **a** Marbled texture and **b** Schlieren texture for nematic phase in Azo-BE on heating and on cooling respectively

### 3.2.1 Electronic properties and QCDs

The energetic nature of the compound is illustrated by the border molecular orbital's plotted for the azo-BE compound (Fig. 12). Benzene ring, nitrogen, sulfur and oxygen atoms were the primary locations for the L, while the H was localized within the structure. This emphasizes how crucial the FMO is for promoting p-p stacking and hydrophobic interactions, causing the chemical and residue receptor chains to engage with each other effectively. The Azo-BE exhibited small energy gaps, indicating polarizability and high reactivity. The parameter values are gathered in Table 1.

Based on the information presented in prior articles on azo compounds (Al-Hamdani et al. 2021c, 2023), we conducted a study on the NLO properties of azo-BE. To investigate these properties, the DFT/B3LYP methods utilized with a 6-311+G(d, p) basis set to generate several QCDs. Our findings indicate that an increase in $E_{HOMO}$, softness (S), and optical softness (So) is indicative of improved NLO properties. Conversely, a decrease in energy gap $E_{LUMO}$, ionization potential IE, and hardness, η, results in increased NLO characteristics. Our synthesized compound demonstrated higher values for $E_{HOMO}$, S, and $S_o$, and lower values for $E_{gap}$, $E_{LUMO}$, and ionization potential IE, suggesting superior NLO properties (Al-Hamdani et al. 2021c, 2022c), Table 1 shows obtained results. The quantitative chemical parameters were computed for the synthesized Azo-BE. The ground-state and excited-state geometries were determined using B3LYP method with 6-311+G(d, p) basis sets. The values of energy of H and L orbitals are found to be 2.3713 and 0.01168 eV, respectively (Table 1). The reduced H–L gap (2.3596 eV) indicate the mechanism of the charge-transfer interaction and show the molecule's chemical activity. The computed QCDs are reported in Table 1 and they exhibit the compound's NLO properties.

### 3.2.2 Analysis of Mulliken population

The calculations of Mulliken atomic charges play a crucial role in quantum chemical of molecular systems, as atomic charges impact key features like molecular polarization and dipole moment (Ebrahimi et al. 2015). In Fig. 13, we observe the atomic charges of Azo-BE, which were obtained using the Mulliken population method. Every hydrogen atom showed

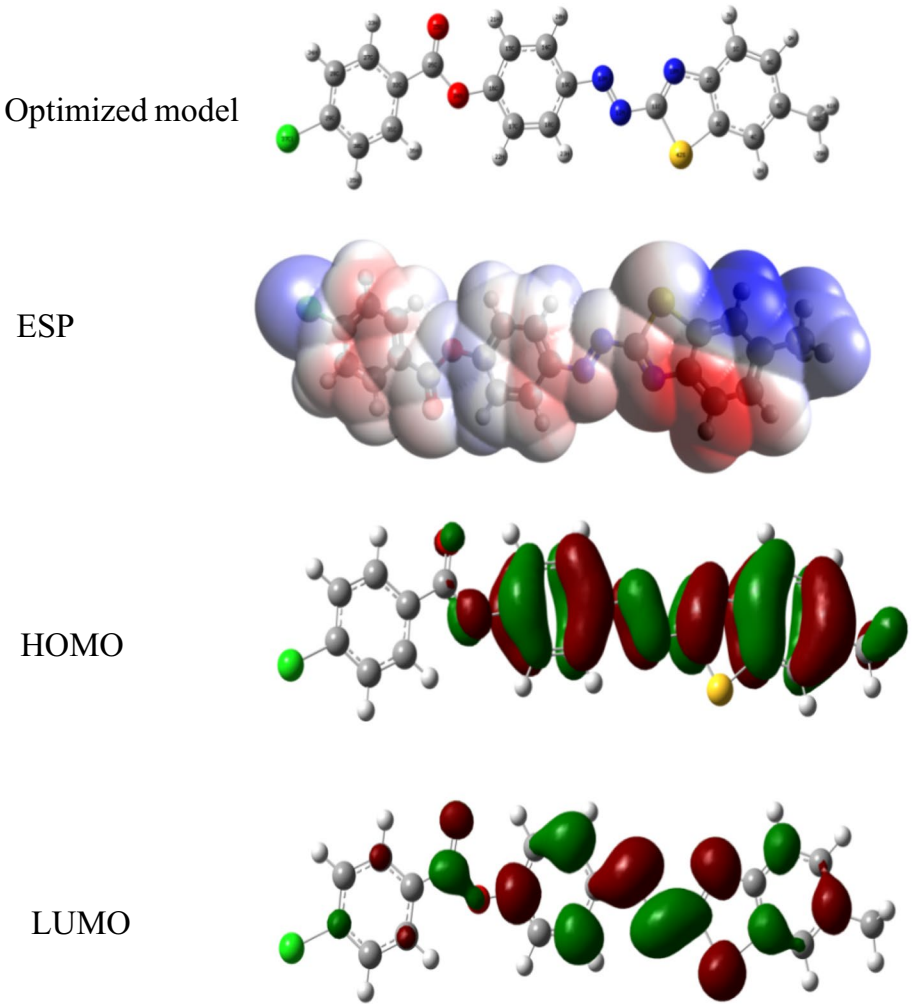


**Fig. 11** The optimized 3D structures (1st row), ESP representations (2nd row), HOMO (3rd row) and LUMO (4th row) orbital's of Azo-BE compound using DFT/ B3LYP/6-311+G(d,p) level

signs of positive charge. Moreover, the Mulliken atomic charges verified that C27–C32 atoms of benzene ring atoms with positive charges owe to inductive effect resulting from presence of an electronegative sulfur atom and carbonyl group, while C2, C3, C9, and C11 atoms have a moderate negative charge due to the distribution of charge between N, O, and S atoms for azo group and the thiazol ring resulting in more reaction sites in these atoms. The other atoms (N10, N12, N13, O24, O25, and S42) are all negative, as one would anticipate.

### 3.2.3 NMR analysis

Using Gaussian 09 program the $^{13}$CNMR chemical shift calculations was carried out, and (GIAO) method (Wolinski et al. 1990) for the sake of comparing experimental and

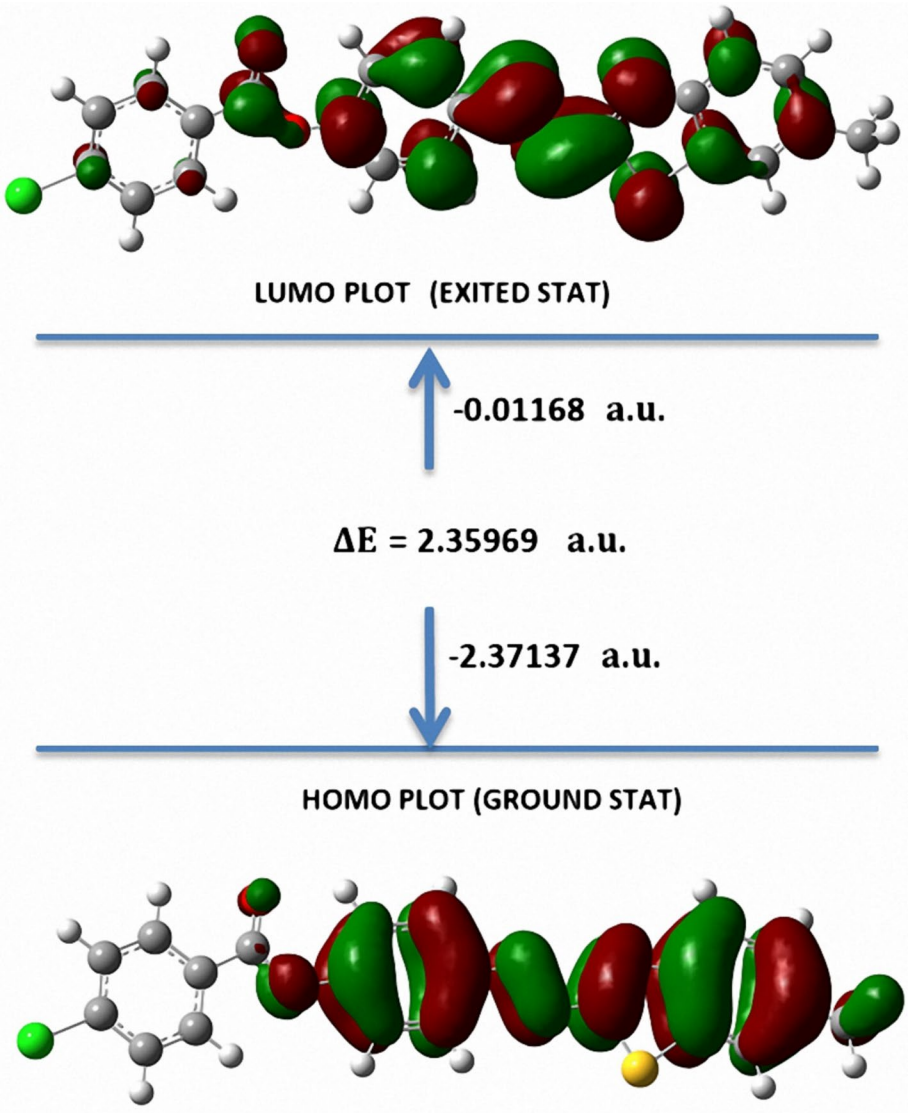


**Fig. 12** The atomic compositions' frontier molecular orbitals (FOM) of Azo-BE determined by DFT/B3LYP/6-311+G(d,p) level

theoretical NMR data. This aid in choosing the right assignments and clarifies how chemical shift and molecular structure are related. To figure out the relation among experimental and the NMR theoretical values chemical shift constants, the experimental data are compared to the estimated values. All carbon atoms' $^{13}$CNMR chemical shifts in the Azo-BE's ideal structures, calculated by the B3LYP method using the 6-311+G(d, p) basis set (Faisal et al. 2022). Each carbon atoms pair at the same location in the molecule was considered as equal, and their chemical shifts were averaged, in order to quantify the $^{13}$CNMR chemical shifts. The statistical properties of calculated $^{13}$CNMR chemical shifts and experimental

**Table 1** Some QCDs of NLO properties

| Parameters | B3LYP |
|---|---|
| $E_{HOMO}$ (eV) | −2.3713 |
| $E_{LUMO}$ (eV) | −0.0116 |
| ΔE (kJ $mol^{-1}$) | 2.3597 |
| $EA = (-E_{LUMO})$ (eV) | 0.0116 |
| $IE = (-E_{HOMO})$ (eV) | 2.3713 |
| $\eta = (IE - EA)/2$ (eV) | 1.1798 |
| $S = (1/\eta)$ $(eV)^{-1}$ | 0.8476 |
| $S_o = (S/2)$ (eV) | 0.4238 |
| $\chi = (IE + EA)/2$ (eV) | 1.1914 |
| $Cp = -\chi$ (eV) | −1.1914 |
| $\omega = (\mu^2/2\eta)$ (eV) | 0.4871 |
| $\mu = (E_{HOMO+} E_{LUMO})/2$ (eV) | −1.1914 |

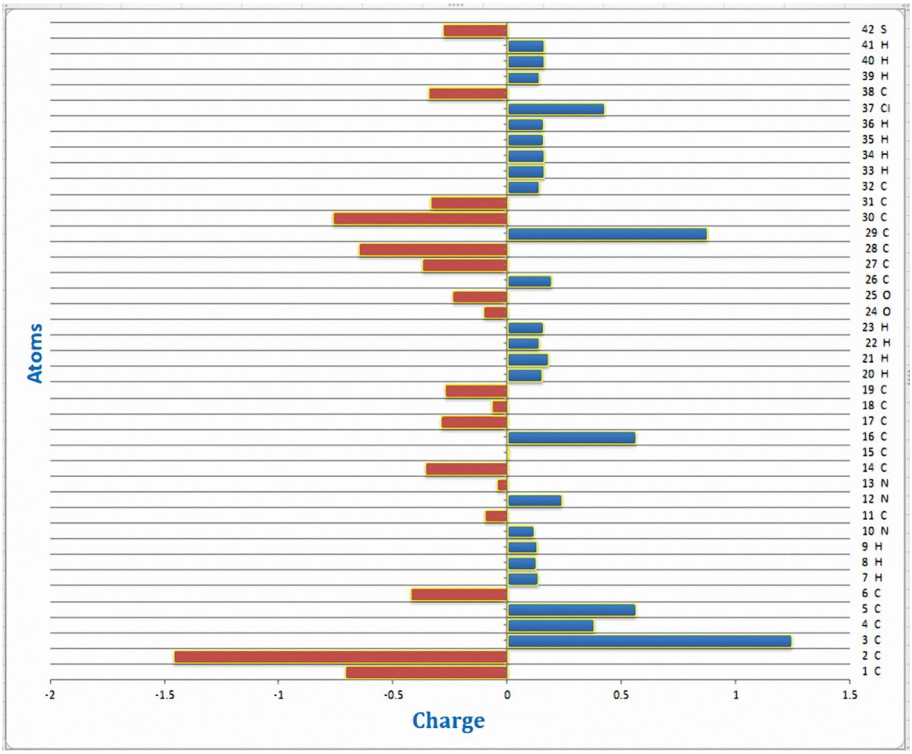


**Fig. 13** The atomic charge distribution for studied Azo-BE according to Mulliken using DFT-B3LYP /6-311+G(d,p)

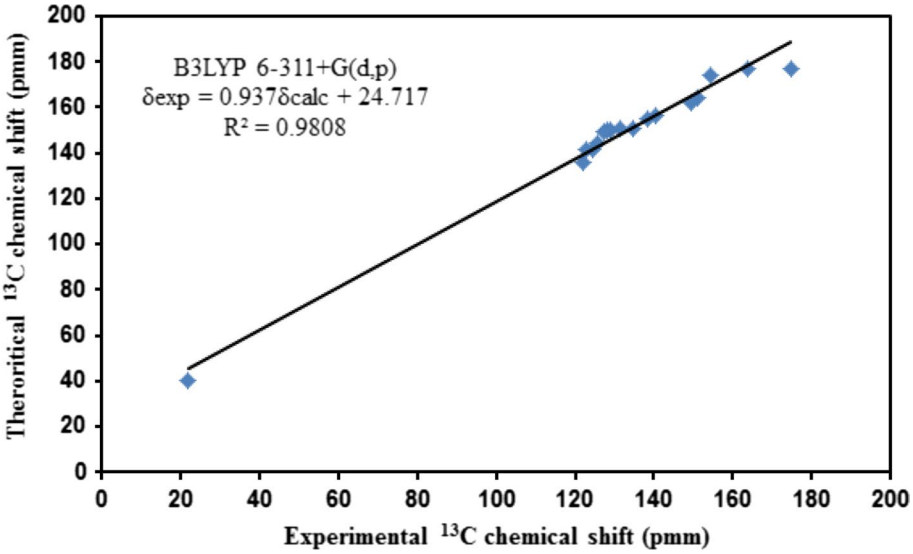


**Fig. 14** Theoretical $^{13}$CNMR chemical shift vs. experimental $^{13}$CNMR values of Azo-BE

detection of azo-BE are shown in Fig. 14. It is evident that the results are in good accord with experimental values.

### 3.2.4 Study the electronic absorption spectrum of indol-3-DMT

The Analytic Shimadzu (UV-160v) spectrometer used to measure the Azo-BE compound absorbance spectrum in the range 300–800 nm. Figure 15 shows the Azo-BE

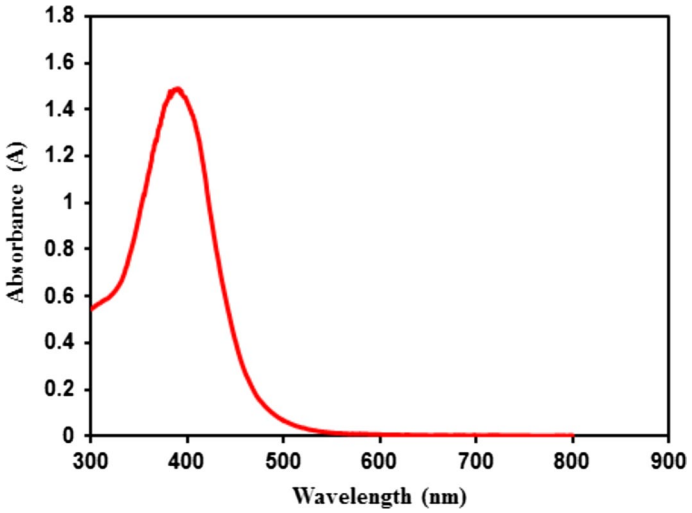


**Fig. 15** UV–Vis absorbance (A) of the Azo-BE

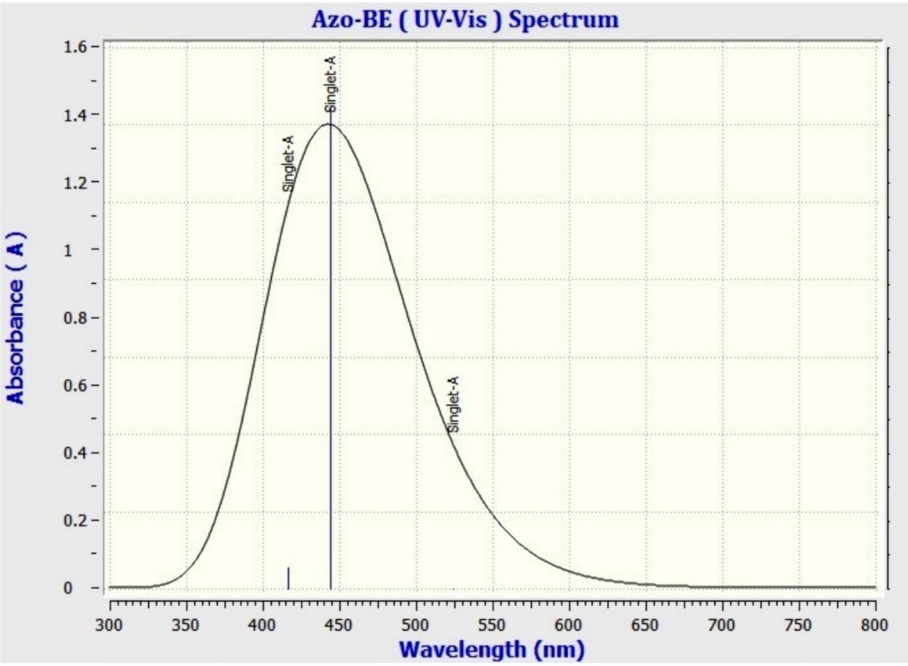


**Fig. 16** The theoretical calculation of electronic spectrum of Azo-BE, was calculated by DFT- B3LYP/6-311+G(d,p)

**Table 2** Theoretical and experimental band maxima, and intensities of Azo-BE, was calculated by DFT-B3LYP/6-311+G(d, p)

| Transitions | Theoretical $\lambda_{max}$ (nm) | Experimental $\lambda_{max}$ (nm) | (*f*) | Experimental oscillator strength ($cm^2$ $Mol^{-1}$) | Transition energy gap (ΔE) eV | Assignment |
|---|---|---|---|---|---|---|
| H→L | 416.74 | Not observed overlapping | 0.0635 | | 3.115 | π–π* |
| H-1→L | 443.77 | 416.9 | 1.4287 | 22,800 | 3.129 | π–π* |
| H-2→L | 524.29 | Not observed overlapping | 0.0000 | | 3.137 | π–π* |

absorbance (A) spectrum. Using the equation mentioned in the study (El-Fadl et al. 2005), the linear absorption coefficient, $\alpha$, is calculated 473 nm and 532 nm, and we found them equal to 3.84 $cm^{-1}$ and 0.55 $cm^{-1}$, respectively.

Theoretical absorption analyses (Fig. 16) were out to examine Azo-BE's NLO characteristics. The results are presented in Table 2, which contains the related computed transitions and *f*. In general, the electronic transition spectrum of a benzothiazole aromatic compound in solution displays two bands of high intensity, one of which can be seen in the visible region and is associated with the electronic π–π* transition of the aromatic ring (Hashim et al. 2024; Belahlou et al. 2023; Sahki et al. 2021).

The calculated absorption bands (using DFT/ B3LYP theory level with 6-311+G(d,p) basis set) for the H → L state are shown at 414.7 nm for the H-1 → L states at 433.7 nm and for the H-2 → L state at 524.29 nm with *f* (oscillator strengths) of 0.0635, 1.4287, and 0.000, respectively (Table 2) as well as the electronic transitions includes elements of the HOMO to LUMO transition are shown in Fig. 17. The f indicates the high likelihood of these transitions occurring. Since the transitions are designated as π–π* transitions, the system is unsaturated, increasing the possibility of an active charge transfer.

### 3.3 DPs

In this part, the following experiments were conducted.

#### 3.3.1 DPs: temporal behavior

This experiment was conducted at constant input power of 54 mW passing through Azo-BE in the 1 mm glass cell. The steady state of the DPs reached in 1 s.

The resulted temporal behavior is shown in Fig. 18. The beam spot on the screen started as small bright initial time 0 ms, that increases in area until it reach's large area with no rings as time lapse due to self-defocusing (SDF). The spot size then breaks into rings whose number increased with time then an asymmetry resulted so that DPs appeared compressed in the upper half due to the thermal convection current that moves upper hot half

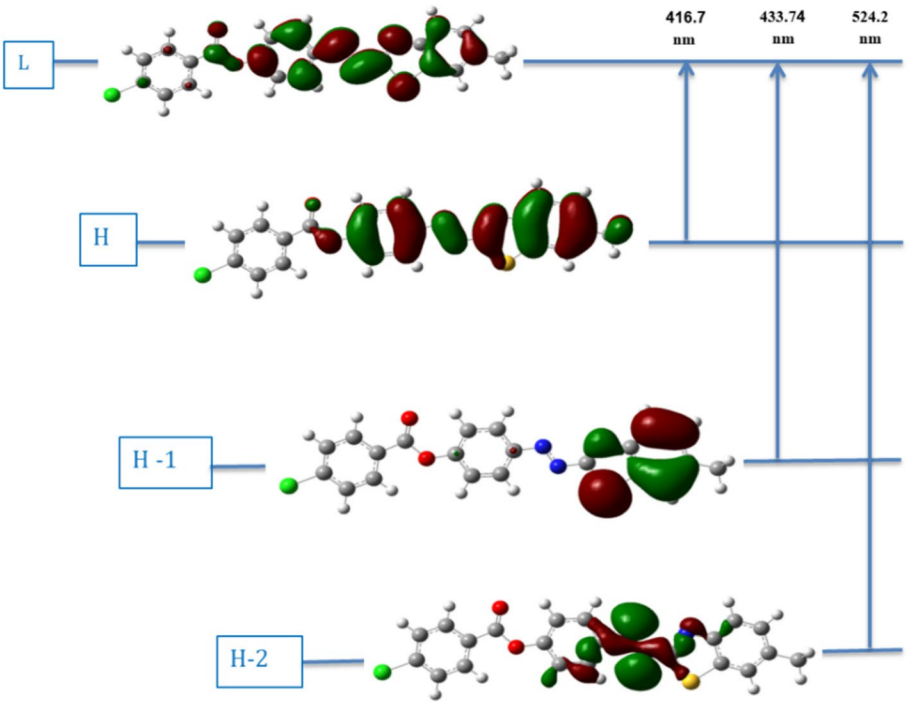


**Fig. 17** Calculation of TD-SCF using DFT/B3LYP theory level with 6-311+G(d, p) basis set for Azo-BE

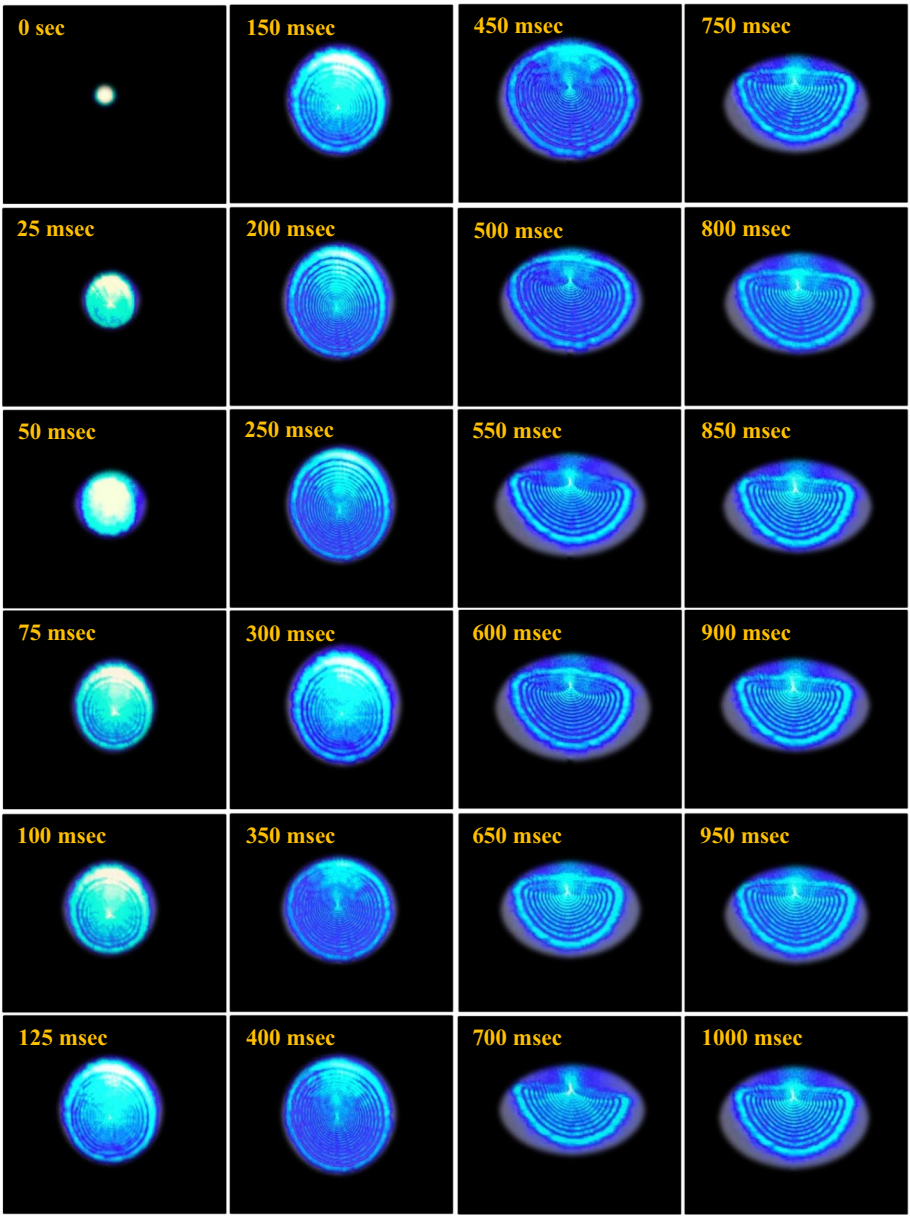


**Fig. 18** DP temporal evolution in Azo-BE at 54 mW

upward which is replaced with another cold one that reduces medium temperature locally hence the beam phase change locally of the beam hence the upper half rings grew in a smaller ratio than low rings.

### 3.3.2 DPs: wave front effect

Wave front effect on the DPs is studied by choosing two types of wave front viz., convergent or divergent when the sample cell fixed before the lens focus and after the lens focus. Such effect was recognized by number of researchers (Santnamto et al. 1984; Deng et al. 2005; Chavez et al. 2008). It is believed by Santamato and Shen that the laser beam interaction with nonlinear material dependent on the sign of the beam wave front radius ($\pm$R), such effect can be noticed in Fig. 19.

### 3.3.3 DPs: power input effect

Power input effect on the type of DPs is shown in Fig. 20. As power input increased, the amount of absorbed energy from the laser beam by the nonlinear medium increased, so does the amount of heat resulted that increases locally the temperature of the nonlinear medium in the shape of Gaussian extent i.e., a negative lens created since the temperature is high at the beam center. The scenario noticed in the sub Sect. 3.3.1 is repeated in this experiment where the DP evolution is the same manner as the one noticed in the sub Sect. 3.3.1.

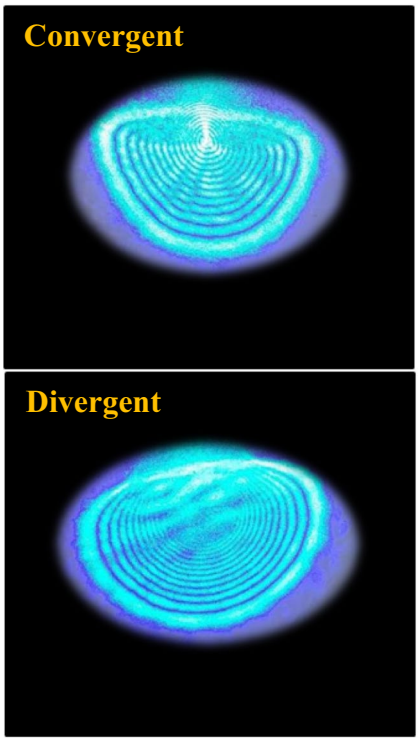


**Fig. 19** Beam wave front dependent of DPs at power input 54 mW in Azo-BE

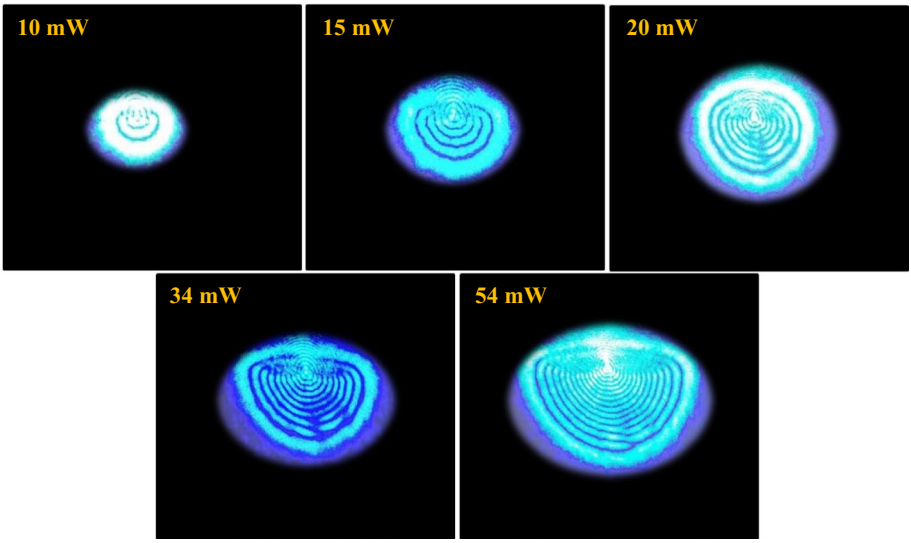


**Fig. 20** Power input dependence by DPs in Azo-BE

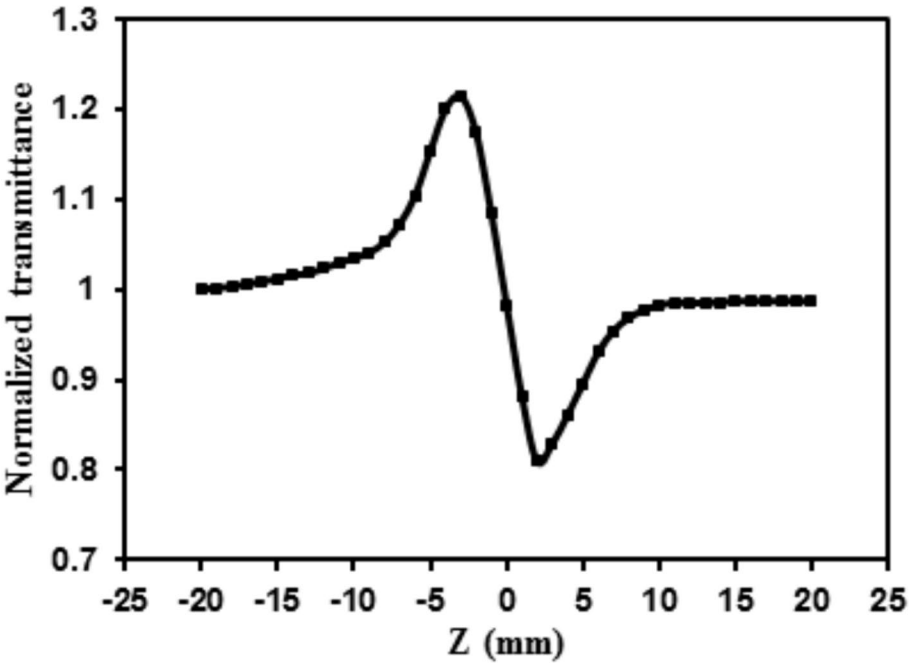


**Fig. 21** CA Z-scan results of Azo-BE

### 3.4 Z-scam

By conducting the standard Z-scans, we can determine the nonlinear absorption coefficient (NLAC), β, and the NLRI, $n_2$, respectively. When conducting OA Z-scan, we obtained a straight horizontal line, which proves that the Azo-BE compound does not bare β. Figure 21 shows the data of CA Z-scan of the Azo-BE. The transmittance peak—valley shape changes with the sample position, z, an indicative of SDF (negative NLRI). Since we use a continuous wave laser beam in the current study, origin of nonlinearity is thermal.

### 3.5 AOS

Two laser beams used in these experiments, and focused, on the sample at the same time. When the 532 nm beam pass through the Azo-BE compound alone, which induced small absorption coefficient ($\alpha = 0.55$ $cm^{-1}$), so that small energy absorbed by the nonlinear medium so that no rings appeared. When the 473 nm beam pass alone, rings appeared, since this beam induced high absorption coefficient ($\alpha = 3.84$ $cm^{-1}$) so that maximum amount of energy absorbed by the nonlinear medium and rings appeared. When both beams simultaneously passes through the nonlinear medium by the cross-passing technique (Jia et al. 2018; Wang et al. 2019; Zhang et al. 2019), two types of DPs resulted one for each beam. The 473 nm beam have effect on the, 532 nm beam, DPs i.e., area, rings number and a symmetry but not their intensity.

The beam 532 nm have effect on its DPs intensity only. The noticed effect is the result of cross self-phase modulation (XSPM) an effect noticed first by Agrawal (Agrawal 1987), Matsuoka et.al. (Matsuoka et al. 1997) and (Jones et al. 2000). The results obtained are shown in Fig. 22. Such AOS refer to as static AOS, since both beams wave of cw character when changing the 473 nm from cw to pulse input resulted from the 473 nm laser keeping the beam 532 nm cw, both pulsed DPs resulted so that we have pulsed or dynamic AOS, as shown in Fig. 23.

### 3.6 Optical limiting

Figure 24a represents the results obtained when conducting the optical limiting experiment. It can be seen from Fig. 20a that the sample has the properties of an optical limiter, where the relation between the input power and output power is linear at low input power, and becomes nonlinear with increasing input power, after that the output power becomes constant as the input power continues increase. To determine the value of the threshold limiting value, we drew a curve between the normalized transmittance and the input power (Fig. 24b), and from a curve, we find that, the value of the threshold limiting equals 16 mW.

### 3.7 Calculating the NLRI, $n_2$

The NERI ($n_2$) of the azo-BE compound was estimated the via DPs and Z-scan.

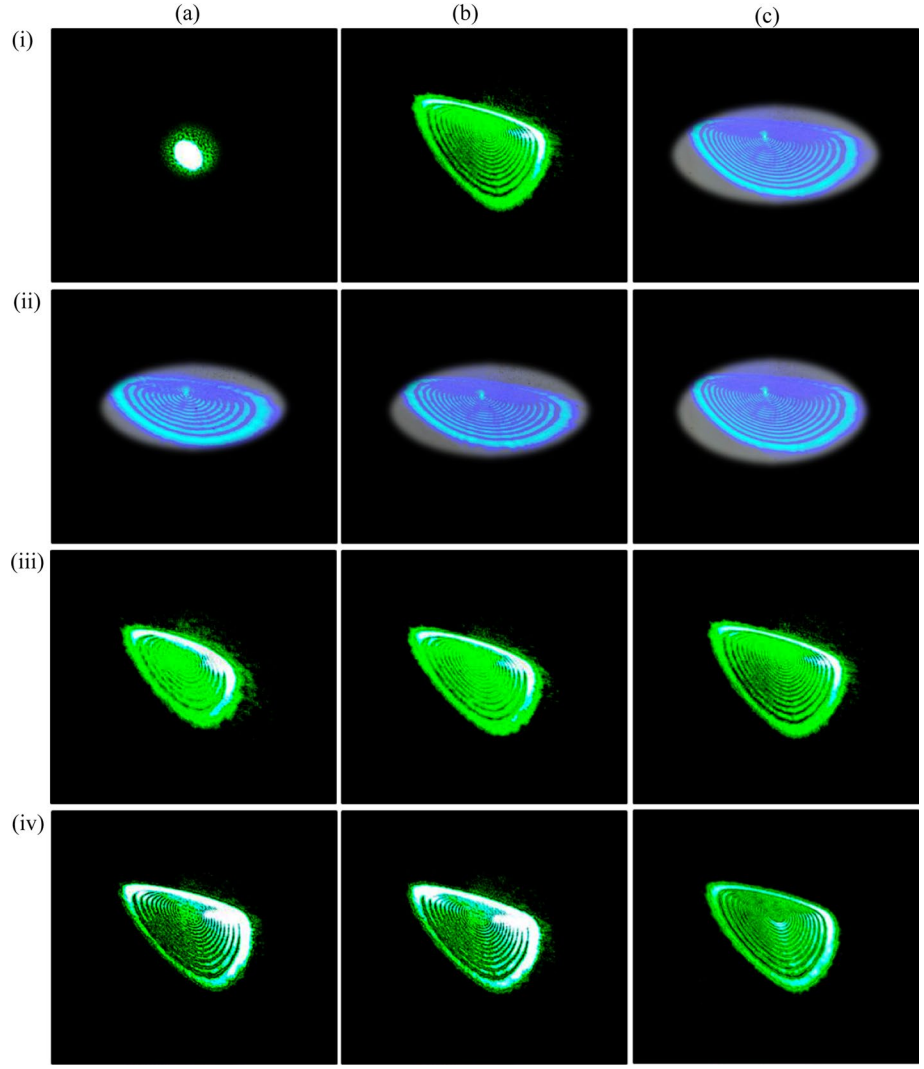


**Fig. 22** Static AOS in the Azo-BE

### 3.7.1 DPs

The $n_2$ of azo-BE compound is estimated using the numbers of DPs resulted when the input power is maximum, $P_{max}$ (Osugu et al. 1996). As the laser beam traverses the sample it enhances a change in it's refractive index (RI), Δn, due to absorbing of part of beam energy dependent on the medium absorption coefficient that leads to an increase of medium temperature. For a sample thickness, d, the change of the medium optical thickness, dΔn, leads to generation of DPs. For one ring to result the beam phase change by an amount of 2π radians. For N rings to result, the total change of the beam phase, $\Delta\varphi$, equals to:

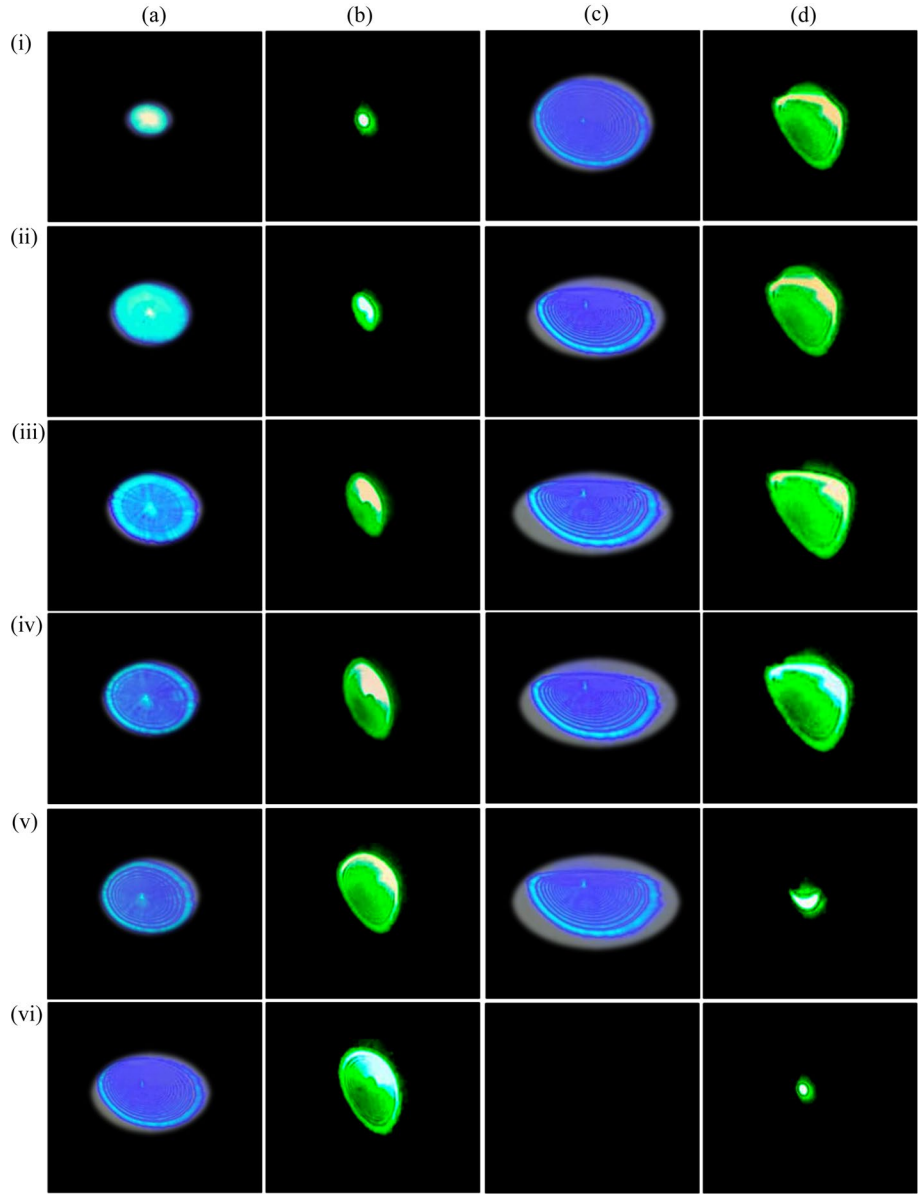


**Fig. 23** Dynamic AOS in Azo-BE

$$\Delta\varphi = 2\pi \mathrm{N} \tag{1}$$

Since the average on-axis RI change leads to phase change, $\Delta\varphi$, equals to $\mathrm{d}\Delta\mathrm{nk}$, were $\mathrm{k} = \frac{2\pi}{\lambda}$ ($\lambda$ is the light wavelength), so that $\Delta\varphi$ can be written once more as:

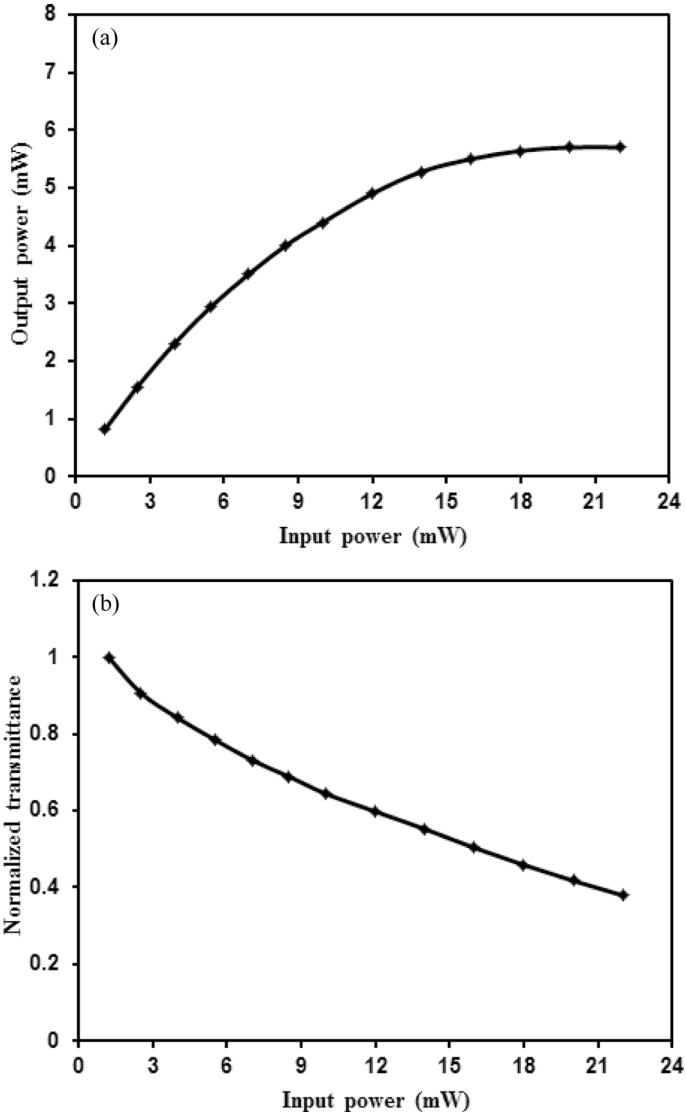


**Fig. 24** **a** Variation of output with input power. **b** Variation of normalized transmittance with input power, in the Azo-BE

$$\Delta\varphi = \Delta nd \cdot \frac{2\pi}{\lambda} \tag{2}$$

so that:

$$\Delta \mathrm{n} = \frac{\mathrm{N}\lambda}{\mathrm{d}} \tag{3}$$

and NLRI ($n_2$) is written as:

$$n_2 = \frac{\Delta n}{I} \tag{4}$$

and for a Gaussian beam the intensity, I, is written as follows:

$$I = \frac{2P}{\pi\omega^2} \tag{5}$$

ω = is the beam radius at the lens focus. For N = 10, λ = 473 nm, d = 1 mm, ω = 19.235 μm, P = 54 mW, I = 9296 W/cm$^2$. i.e., Δn = $4.73 \times 10^{-3}$ and $n_2 = 4.878 \times 10^{-11}$ m$^2$/W.

### 3.7.2 Z-scan

Based on the nonlinearity shown by the sample, which is of thermal origin, $n_2$ is given by the following relation (Sendhil et al. 2006):

$$n_2 = \frac{\Delta T_{p-v}\lambda}{4\pi dI} \tag{6}$$

$$\Delta T_{p-v} = T_p - T_v \tag{7}$$

$T_p$, peak transmittance; $T_v$, valley transmittance.

The value of $\Delta T_{p-v}$ can be obtained from Fig. 18, and by using that value in Eq. 6, we can find the value of $n_2$ of Azo-BE compound, which is equals to $0.22 \times 10^{-11}$ m$^2$/W.

The studied material nonlinearities can be well compared with those studied by Jeyaram et al., such as Schiff base E-N′-(4-(dimethylamino)benzylidene) isonicotinohydrazide (Sudha et al. 2023a), isoniazid-vanillin hybrid Sudha et al. 2023b), and acid blue 129 dye in polar solvents Jeyaram 2024b).

## 4 Conclusion

The compound ((6-methylbenzo[d]thiazol-2-yl)diazenyl)phenyl 4-chlorobenzoate (Azo-BE) was synthesized and characterized via $^1$HNMR, $^{11}$CNMR, mass spectra, etc. The Azo-BE shows nematic phase only and turned into a liquid phase using polarized microscope. We noticed that heating of the nematic phase in the azo gives Marbled texture while cooling took the form of Schlieren. The B3LYP with 6-311+G(d,p) bases set prove the geometrical optimization yield, HOMO–LUMO orbital at potential surface for the nonpolar structure.. The passage of a cw 473 nm wavelength laser beam through the Azo-BE led to the generation of diffraction patterns (DPs). Based on the number of rings at maximum power input. The deformation of the beam wave front let the Z-scan technique used to measure NLIR and the nonlinear absorption coefficient (NLAC). The closed aperture (CA) Z-scan, used to measure the nonlinear refractive index (NLIR) of the Azo-BE was estimated. Azo-BE bare no nonlinear absorption coefficient (NLAC). The all-optical switching (AOS) phenomena both static and dynamic are tested using two laser beams of wavelengths 473 nm and 532 nm.

**Author contributions** Uhood J. Al-Hamdani and Qusay M.A. Hassan wrote the manuscript and analysis of the results, Ayat K. Hashim and H. A. Sultan participated in the characterization, T. A. Alsalim wrote the manuscript, C. A. Emshary wrote the main manuscript text—review and editing.

**Funding** No funding was received for this study.

**Data availability** The authors confirm that the data supporting the findings of this study are available within the article.

## Declarations

**Competing interest** The authors declare that they have no known competing financial interests.

**Ethics approval** The authors declare that their commitment to ethics related to his work and they have designed the experiments, collected and analyzed the data, and written the manuscript.

**Consent for publication** The authors declare their consent of publication.

## References

Adil, A., Hassan, Q.M.A., Alsalim, T.A., Sultan, H.A., Al-Asadi, R.H., Emshary, C.A.: Synthesis, theoretical properties using DFT method, and nonlinear optical properties of 4-methyl umbelliferone derivative. Optik **290**, 171320 (2023)

Agrawal, G.P.: Modulation instability induce by cross-phase modulation. Phys. Rev. Lett. **59**, 880–883 (1987)

Ahmad, H.A., Hagar, M., Alhaddad, O.A., Zaki, A.A.: Optical and geometrical characterizations of nonlinear supramolecular liquid crystal complexes. Crystals **10**, 701 (2020)

Al-Hamadani, U.J., Gassim, T.E., Radhy, H.H.: Synthesis and characterization of azo compounds and study of the effect of substituents on their liquid crystalline behavior. Molecules **15**, 5620–5628 (2010)

Al-Hamadani, U.J., Hassan, Q.M.A., Emshary, C.A., Sultan, H.A., Dhumad, A.M., Al-Jaber, A.A.: All optical switching and the optical nonlinear properties of 4-(benzothiazolyldiazenyl)-3-chlorophenyl 4-(nonylthio)benzoate (EB-3Cl). Optik **248**, 168196 (2021a)

Al-Hamadani, U.J., Jassem, A.M., Dhumad, A.M., Al-Shlshat, S.: Synthesis mesomorphic properties and theoretical study of benzothiazole-aromatic molecules with ester-and azomethine-linking groups. Liq. Cryst. **48**, 2164–2177 (2021b)

Al-Hamadani, U.J., Shihabaldain, N.L., Al-Mayah, D.S., Jassem, A.M.: Influence of different linkages on the mesomorphic properties of aromatic ring system liquid crystals. Mol. Cryst. Liq. Cryst. **725**, 13–24 (2021c)

Al-Hamadani, U.J., Abbo, H.S., Fadhl, A.A., Titinchi, S.J.J.: Chloro-benzothiazole Schiff base ester liquid crystals: synthesis and mesomorphic investigation. Liq. Cryst. **49**, 1866–1877 (2022a)

Al-Hamadani, U.J., Abdulwahhab, H.A., Hussein, K.A.: Effects of terminal substituents on mesomorphic properties of Schiff base–ester mesogens and DFT calculations. Liq. Cryst. **49**, 1998–2007 (2022b)

Al-Hamadani, U.J., Hassan, Q.M.A., Zaidan, A.M., Sultan, H.A., Hussain, K.A., Emshary, C.A., Alabullah, Z.T.Y.: Optical nonlinear properties and all optical switching in a synthesized liquid crystal. J. Mol. Liq. **361**, 119676 (2022c)

Al-Hamadani, U.J., Hassan, Q.M.A., Elias, R.S., Sultan, H.A., Alshishat, S.A., Emshary, C.A.: Thermal nonlinearity and all-optical switching of synthesized Azo-Cl compound. Opt. Mater. **139**, 113824 (2023)

Aljamali, N.M., Al-Qraawy, W.K.N., Asd, M.G., Almosawy, A.: Review on liquid crystals and their chemical applications. Cheminfo. Res. **7**, 8–13 (2021)

Almashal, F.A., Mohammed, M.Q., Hassan, Q.M.A., Emshary, C.A., Sultan, H.A., Dhumad, A.M.: Spectroscopic and thermal nonlinearity study of a Schiff base compound. Opt. Mater. **100**, 109703 (2020)

Alrefaee, S.H., Ahmad, H.A., Khan, M.T., Al-Ola, K.A., Al-Refai, H., El-Atawy, M.A.: New self-organizing optical materials and induced polymorphic phases of their mixtures targeted for energy investigations. Polymers **14**, 456 (2022)

Ara, M.H.M., Bahramian, R., Mousavi, S.H., Abolhasan, M.: Self-phase modulation and ring pattern observation by applying electrical field on dye-doped nematic liquid crystal. J. Mol. Liq. **149**, 18–21 (2004)

Ara, M.H.M., Mousavi, S.H., Koushki, E., Salmani, S., Ghaibi, A., Gilani, A.G.: Nonlinear optical respondes of sudan IV doped liquid crystal by Z-scan and moire deflectometry techniques. J. Mol. Liq. **142**, 29–31 (2008)

Beeckman, J., Nuyts, K., Vanbrabant, P.J.M.: Liquid-crystal photonic applications. Opt. Eng. **50**, 081202 (2011)

Belahlou, H., Abed, S., Bouchouit, M., Taboukhat, S., Messaadia, L., Bendeif, E., Bouraiou, A., Sahraoui, B., Bouchouit, K.: Molecular structure, computational studies and nonlinear optical properties of a new organic chalcone crystal. J. Mol. Struct. **1294**, 136488 (2023)

Bighan KJ (2018) LCP interaction to liquid crystal polymer ZEUS, 2016, 20 pp

Bunjes, H., Rades, T.: Thermo tropic liquid crystalline drugs. Pharma Pharma **57**, 807–816 (2005)

Castellano, J.A.: Liquid crystal display applications, past, present and future. Liq. Cryst. Today **1**, 4–6 (1990)

Chavez-Cerda S, Nascimento CM, Alencar MARC, Silva MLAD , Meneghetti MR, Hickmann JM (2008) Expermintal observation of The fare field diffraction patterns of divergent and convergent Gaussian beams in a self-defocusing medina. In: Annals of Optics XXIX ENFMC, pp. 1–6

Cuppo, F.L.S., Neto, A.M.F., Gomez, S.L.: Thermal lens compared with the sheik-Bahae formalism in interpreting Z-scan experiments on lyotropic liquid crystals. J. Opt. Soc. Am. B **19**, 1342–1348 (2002)

Deepa, C., Jeyaram, S.: Facile Z-scan determination of nonlinear refractive index and absorption coefficient of dye-doped polymer film. Bull. Mater. Sci. (2024). https://doi.org/10.1007/s12034-024-03150-2

Deepa, C., Madhu, S., Devasenan, S., Mural, G., Pancharatna, P.D., Maaza, M., Kaviyarasu, K., Jeyaram, S.: Extraction of natural pigment curcumin from curcuma longa: Spectral, DFT, third-order nonlinear optical and optical limiting study. Accepted for publication in a J. Fluoresc. (2023). https://doi.org/10.1007/s10895-023-03421-x

Deng, L., He, K., Zhou, H., Li, C.: Formation and evolution of far-field diffraction pattern of divergent and convergent Gaussian beams Rassing through self-focusing and self-defocusing medium. I-Opt A Pure Appl Opt **7**, 409–415 (2005)

Dhumad, A.M., Hassan, Q.M.A., Emshary, C.A., Fahad, T., Raheem, N.A., Sultan, H.A.: Nonlinear optical properties investigation of a newly synthesised Azo-(β)- diketone dye. J. Photochem. Photobiol. A Chem. **418**, 113429 (2021a)

Dhumad, A.M., Hassan, Q.M.A., Fahad, T., Emshary, C.A., Raheem, N.A., Emshary, C.A., Sultan, H.A.: Synthesis, structural characterization and optical nonlinear properties of two azo-β-diketones. J. Mol. Struct. **1235**, 130196 (2021b)

Durbin, S.D., Arakelian, S.M., Shen, Y.R.: Laser-induced diffraction rings from a nematic liquid-Crystal fi(ms). Opt. Lett. **6**, 411–413 (1981)

Ebrahimi, H.P., Hadi, J.S., Alsalim, T.A., Ghali, T.S., Bolandnazar, Z.: A novel series of thiosemicarbazone drugs: from synthesis to structure. Spectrochimi Acta Part A Mol Biomol Spectroscopy **137**, 1067–1077 (2015)

El-Fadl, A.A., Mohamad, G.A., El-Moiz, A.B.A., Rashad, M.: Optical constants of Zn1−xLixO films prepared by chemical bath deposition technique. Phys. B **366**, 44–54 (2005)

Elias, R.S., Hassan, Q.M.A., Sultan, H.A., Al-Asadi, A.S., Saeed, B.A., Emshary, C.A.: Thermal nonlinearities for three curcuminoids measured by diffraction ring patterns and Z-scan under visible CW laser illumination. Opt. Las. Technol. **107**, 131–141 (2018)

Faisal, A.G., Hassan, Q.M.A., Alsalim, T.A., Sultan, H.A., Kamounah, F.S., Emshary, C.A.: Synthesis, optical nonlinear properties, and all-optical switching of curcumin analogues. J. Phys. Org. Chem. **e4401**, 1–16 (2022)

Gomez, S.L., Cuppo, F.L.S., Neto, A.M.F.: Nonlinear optical properties of liquid crystals propped by Z-scan technique. Braz. J. Phys. **33**, 813–820 (2003)

Hashim, Z., Hassan, Q.M.A., Alsalim, T.A., Sultan, H.A., Emshary, C.A.: Synthesis, spectral, and NLO studies of indol derivative bearing 1, 2, 4-triazole-3-thiol group. Opt. Mater. **153**, 115582 (2024)

Hassan, Q.M.A., Sultan, H.A., Al-Asadi, A.S., Kadhum, A.J., Hussein, N.A., Emshary, C.A.: Synthesis, characterization, and study of the nonlinear optical properties of two new organic compounds. Synth. Metal. **257**, 116158 (2019)

Hassan, Q.M.A., Raheem, N.A., Emshary, C.A., Dhumad, A.M., Sultan, H.A., Fahad, T.: Preparation, DFT and optical nonlinear studies of a novel azo-(β)-diketone dye. Opt. Laser Technol. **148**, 107705 (2022)

Janossy, I., Szabados, L.: Photoisomerization of azo-dyes in nematic liquid crystals. J. Nonlinear Opt. Phys. Mater. **7**, 539–551 (1998)

Jassem, A.M., Hassan, Q.M.A., Almashal, F.A., Sultan, H.A., Dhumad, A.M., Emshary, C.A., Albaaj, L.T.T.: Spectroscopic study theoretical calculations and optical nonlinear properties of amino acid (glycine)-4-nitro benzaldeyhyde-derived Schiff base. Opt. Mater. **122**, 111750 (2021a)

Jassem, A.M., Hassan, Q.M.A., Emshary, C.A., Sultan, H.A., Almashal, F.A., Radhi, W.A.: Synthesis and optical nonlinear properties performance of azonaphthol dye. Phys. Scr. **96**, 025503 (2021b)
Jeyaram, S.: Study of third-order nonlinear optical properties of basic violet 3 dye in polar protic and aprotic solvents. J. Fluorescopy **31**, 1637–1644 (2021a)
Jeyaram, S.: Intermolecular charge transfer in donor–acceptor substituted triarylmethane dye for NLO and optical limiting applications. J. Mater. Sci. Mater. Electron. **32**, 9368–9376 (2021b)
Jeyaram, S.: Nonlinear absorption features of acid blue 129 dye in polar solvents: role of solvents on solute molecule. J. Fluorescopy **34**, 313–320 (2024b)
Jeyaram, S.: Low-power Z-scan study of nonlinear refractive index and absorption coefficient of acid blue 129 dye-doped polymer thin film. Accepted for publication in a Bull. Mater. Sci. **47**, 75 (2024a). https://doi.org/10.1007/s12034-024-03143-1
Jia, Y., Shan, Y., Wu, L., Dai, X., Fan, D., Xiang, Y.: Broadband nonlinear optical resonances and all-optical switching of Liquid phase exfoliated tungsten diselenide. Photon. Res. **6**, 1040–1047 (2018)
Jones, D.J., Diddams, S.A., Taubman, M.S., Cundiff, S.T., Ma, L.S., Hall, J.L.: Frequency comb generation using femtosecond pulses and cross-phase modulation in optical fiber at arbitrary center frequencies. Opt. Lett. **25**, 308–310 (2000)
Kadhum, A.J., Hussein, N.A., Hassan, Q.M.A., Sultan, H.A., Al-Asadi, A.S., Emshary, C.A.: Investigating the nonlinear behavior of cobalt (II) phthalocyanine using visible CW laser beam. Optik **157**, 540–550 (2018)
Khoo, I.C.: Liquid crystal nonlinear optics. Phys. Polo. A **86**, 267–278 (1994)
Lin, Y.J., Zhang, Y.B., Shi, J., Huang, H., Walker, T.R., Huang, T.J.: Optically switchable gratings based on azo-dye-doped polymer-dispersed liquid crystals. Opt. Lett. **34**, 2351–2353 (2009)
Lukishova, S.: Nonlinear optical respond by cyanobiphenyl liquid crystals to high-power nanosecond laser radiation. I. Nonl. Opto. Phys. Mater. **9**, 365–411 (2000)
Matsuoka, S., Miyanaga, N., Amano, S., Nakatsuka, M.: Frequency modulation controlled by cross-phase modulation in optical fiber. Opt. Lett. **22**, 25–27 (1997)
Mitov, M.: Liquid crystal science from 1888 to 1922: Building revolution. Chem. Phys. Chem. **15**, 1245–1250 (2014)
Mousavi, S.H., Koushki, E., Haratizadeh, H.: Nonlinear optical investigation of Gaussian laser beam propagating in a dye-doped nematic liquid crystal. J. Mokee Liq. **153**, 124–128 (2010)
Mutlaq, D.Z., Hassan, Q.M.A., Sultan, H.A., Emshary, C.A.: The optical nonlinear properties of a new synthesized azo-nitrone compound. Opt. Mater. **113**, 110815 (2021)
Ogusu, K., Kohtani, Y., Shao, H.: Laser induced diffraction rings from an absorbing solution. Opt. Rev. **3**, 232–234 (1996)
Okutan, M., San, S.E., Koysal, O., Yakuphanoglu, F.: Investigation of refractive index dispersion and electrical properties in carbon nano-balls' doped nematic liquid crystals. Phys. B **362**, 180–186 (2005)
Prakash, J., Jeyaram, S.: Synthesis, characterization morphological linear and nonlinear optical properties of silicon carbide doped PVA nanocomposites. SILICON **14**, 11163–11170 (2022)
Rajak, P., Nath, L.K., Bhuyan, B.: Liquid-crystals: An approach in drug delivery. Ind. J. Pharmacen. 11–21(2019)
Saeed, B.A., Hassan, Q.M.A., Emshary, C.A., Sultan, H.A., Elias, R.S.: The nonlinear optical properties of two dihydropyridones derived from curcumin. Spectrochim. Acta Part A Mol. Biomol. Spectroscopy **240**, 118622 (2020)
Sahki, F.A., Bouraiou, A., Taboukhat, S., Messaadia, L., Bouacida, S., Figa, V., Bouchouit, K., Sahraoui, B.: Design and synthesis of highly conjugated electronic phenanthrolines derivatives for remarkable NLO properties and DFT analysis. Optik **241**(15), 166949 (2021)
Salim, J.K., Hassan, Q.M.A., Jassem, A.M., Sultan, H.A., Dhumad, A.M., Emshary, C.A.: An efficient ultrasound-assisted CH3COONa catalyzed synthesis of thiazolidinone molecule: theoretical and nonlinear optical evaluations of thiazolidinone-Schiff base derivative. Opt. Mater. **133**, 112917 (2022)
Santamato, E., Shen, Y.R.: Field curative effect on the diffraction ring pattern of laser beam dressed by spatial-self-phase modulation in nematic film. Opt. Lett. **9**, 564–568 (1984)
Sendhil, K., Vijayan, C., Kothiyal, M.P.: Low-threshold optical power limiting of cw laser illumination based on nonlinear refraction in zinc tetraphenyl porphyrin. Opt. Laser Technol. **38**, 512–515 (2006)
Sierakowski, M.: Nonlinear liquid crystalline optical cells. Opt. Appl. **XXIV**, 219–224 (1994)
Song, L., Lee, W.K.: Laser induced self- phase modulation in nematic crystals and effects of applied dc electric field. Opt. Commun. **259**, 293–297 (2006)
Sudha, N., Surendran, R., Jeyaram, S.: Low power Z-scan studies of Schiff base E-N'-(4-(dimethylamino) benzylidene) isonicotinohydrazide for nonlinear optical applications. Ind. J. Phys. **97**, 4399–4408 (2023a)

Sudha, N., Surendran, R., Jeyaram, S.: Vibrational spectroscopic, structural, linear and third order nonlinear optical properties of ionized-vanillin hybrid. Ind. J. Phys. **98**, 1453–1462 (2023b)
Sultan, H.A., Hassan, Q.M.A., Al-Asadi, A.S., Elias, R.S., Bakr, H., Saeed, B.A., Emshary, C.A.: Far-field diffraction patterns and optical limiting properties of bisdemethoxycurcumin solution under CW laser illumination. Opt. Mater. **85**, 500–509 (2018)
Sultan, H.A., Dhumad, A.M., Hassan, Q.M.A., Fahad, T., Emshary, C.A., Raheem, N.A.: Synthesis, characterization and the nonlinear optical properties of newly synthesized 4-((1,3-dioxo-1-phenylbutan-2-yl) diazenyl) benzenesulfonamide. Spectrochimi. Acta. Part A Mol. Biomol. Spectroscopy **251**, 119487 (2021)
Tuma, F.A., Ashoor, M.J., Sultan, H.A., Al-Saymari, F.A., Hassan, Q.M.A., Alsalim, T.A., Emshary, C.A., Saeed, B.A.: Curcumin analogue spectral, nonlinear optical properties and all-optical switching using visible, low power cw laser beams. J. Fluorescopy (2023). https://doi.org/10.1007/s10895-023-03475-x
Vinitha, G., Ramalingam, A.: Single-beam Z-scan measurement of the third-order optical nonlinearities of triarylmethane dyes. Laser Phys. **18**, 1176–1182 (2008)
Wang, Q., Wu, X., Wu, L., Xiang, Y.: Broadband nonlinear optical response in $Bi_2$, $se_3$-$Bi_2$ $Te_3$ heteros fracture and its application in all-optical Switching. AIP Adv. **9**, 025022 (2019)
Wee, I.T., Shahi, J., Ramteke, V., Syed, I.: Liquid crystals pharmacenical application: a review. Int. J. Pharm. Res. All. Sci. **1**, 06–11 (2012)
Wen, Z.B., Shaw, R.F., Raquez, J.M., Clark, N.A., Yang, K.K., Wang, Y.Z.: Unique two-way free-standing thermy-and photo responsive shape memory azobenzone-containing polyurethane liquid crystal network. Sci. China Mater. **63**, 2590–2598 (2020)
Wolinski, K., Hilton, J.F., Pulay, P.: Efficient implementation of the gauge-independent atomic orbital method for NMR chemical shift calculations. J. Am. Chem. Soc. **112**, 8251–8260 (1990)
Zhang, X.J., Yuan, Z.A., Yang, R.X., He, Y.C., Qin, Y.I., Xiao, S., He, J.: A review on spatial self-phase modulation of two-dimensional materials. J. Cent. South Univ. **26**, 2295–2306 (2019)
Zhao, Y.: New photoactive polymer, and liquid-crystal materials. Pure Appl. Chem. **76**, 1499–1508 (2004)
Zolot'ko, A.S., Kitaeva, V.F.: Quantities: periodic structures in multicomponent mixtures of nematic liquid crystals in the region of the nematic liquid-crystal-isotropic liquid phase transition. JETP Lett. **62**, 125–129 (1995)
Zolot'ko, A.S., Kitaeva, V.F., Kitaeva, V.F., Sobolev, N.N., Chillag, L.: The effect of an optical field on the nematic phase of the liquid crystal OCBP. JETP Lett. **32**, 158–161 (1980)